پژوهشگاه نیرو

مرکز توسعه فناوری ابررسانا

پاییز ۱۳۹۸

- همایش‌ها، سمینارها، کنفرانس‌ها و نمایشگاه‌ها
- پروژه ها
- پروژه‌های پایلوت
- گزارش جلسات

بروندادهای تخصصی مرکز تخصصی فناوری ابررسانا، با هدف فراهم نمودن بستری مناسب برای تبادل اطلاعات به صورت داخلی منتشر می‌شود.

مدیر مسئول: مهندس حسین کوهانی

همکاران این شماره: دکتر نسترن ریاحی نوری، دکتر حسام فلاح آرانی، دکتر نرجس باقری، مهندس پریسا جبارنژاد، مهندس نازنین عبدی

ناشر: مرکز فناوری ابررسانا پژوهشگاه نیرو

نشانی الکترونیکی: superconductor@nri.ac.ir nabdi@nri.ac.ir

نشانی: تهران، شهرک غرب، انتهای پونک باختری، پژوهشگاه نیرو، گروه پژوهشی مواد غیرفلزی

فهرست مطالب

خلاصه جلسات برگزار شده

بازنگری سند توسعه فناوری ابررسانا در صنعت برق

جلسات "بازنگری سند توسعه فناوری ابررسانا در صنعت برق" کار خود را با حضور مجری طرح، مدیر پروژه و ناظر بیرونی طرح آغاز به کار نموده است و تاکنون دو جلسه برگزار گردیده است و مواردی جهت بازنگری سند مطرح و به تصویب اعضا جلسه رسیده است که از جمله می توان به استفاده از مشاور به منظور مدیریت فناوری اشاره نمود.

جلسات RIP

با توجه به دو مشخصه اصلی ابررسانایی یعنی مقاومت تقریباً صفر در مقابل عبور جریان الکتریکی و نفوذ ناپذیری مغناطیسی، مواد ابررسانا کاربردهای بالقوه فراوانی از جمله سیم‌ها و کابل‌ها، ترانسفورماتورها، موتورها و ژنراتورها، ذخیره سازهای مغناطیسی، محدود سازهای جریان خطا، سوئیچ ها می‌توانند داشته باشند.

تحقق استفاده از ابررساناها دستاوردهایی همچون جلوگیری از هدر رفتن انرژی در انتقال و دستگاه‌های مصرف کننده، کاهش آلودگی‌های زیست محیطی در اثر کاهش روغن‌های مصرفی در تجهیزات، پایداری هرچه بیشتر سیستم‌های انتقال، امکان ذخیره‌سازی انرژی در هنگام کاهش مصرف، امکان انتقال انرژی‌های پراکنده، امکان استفاده از منابع انرژی سیار چون باطری به مدت‌های طولانی، جلوگیری از آسیب‌های واده بعلت ماهیت محدود کنندگی ابررساناها و گسترش و توسعه شهرسازی بعلت زیرزمینی بودن ابررساناها وکاهش موانع در اثر حذف کابل‌های هوایی رابرای کشور به همراه خواهد داشت.

متخصصین فعال در زمینه ابررسانا، در یکی از جلسات RIP که با حضور مسئولین و محققین پژوهشگاه برگزار گردید، گزارشی از فعالیت های تحقیقاتی خود را در زمسنه ابررسانا ارائه نمودند. در این جلسه به بررسی زوایای مختلف طرحهای زیر پرداخته شد.

تسلط به دانش فنی طراحی و ساخت تجهیزات (کابل، ترانسفورماتور و محدودساز جریان خطا و ذخیره‌ساز و ...) در دمای پایین جهت استفاده در تجهیزات با اولویت مبتنی بر ابررسانا (آزمایشگاهی، نیمه‌صنعتی و صنعتی)

تسلط به دانش فنی طراحی و ساخت سیستم‌های خنک‌کن و عایق‌بندی (آزمایشگاهی، نیمه‌صنعتی و صنعتی) در دمای پایین جهت استفاده در تجهیزات با اولویت مبتنی بر ابررسانا

" تسلط به دانش فنی طراحی و ساخت پودر، سیم و نوار ابررسانای دما بالا" پروژه های خاتمه یافته مرتبط و اقدامات، چالش ها و مشکلات پرداخته شد.

کنفرانسهای بین المللی مرتبط با ابررسانا

10th Asian Cryogenic and Applied Superconductivity Conference - 2nd International Cryogenic Materials Conference in Asia

"دهمین کنفرانس سرمازایی و کاربرد ابررسانا[۱]" و "دومین کنفرانس مواد سرمازایی در آسیا[۲]"، توسط جامعه ابررسانی و سرمازایی ژاپن، در اکیناوا ژاپن در تاریخ ششم تا نهم ۲۰۲۰، برگزار خواهد شد. همچنین چهارمین مدرسه تابستانی ابررسانایی آسیا در ششم ژانویه برگزار خواهد شد. آخرین تاریخ ارسال مقاله، هشت اکتبر ۲۰۱۹ می باشد.

[۱] 2nd International Cryogenic Materials Conference in Asia (Asian-ICMC)

[۲] the 10th Asian Cryogenics and Applied Superconductivity Conference (ACASC)

Modelling of High Temperature Superconductors (HTS)

هفتمین ورکشاپ بین المللی در زمینه مدل سازی ابررساناهای دما بالا، از تاریخ ۲۶ام تا ۲۹ام سال ۲۰۲۰ میلادی، در نانسی فرانسه برگزار خواهد شد. اطلاعات تکمیلی در این زمینه را می توان در آدرس اینترنتی زیر پیدا نمود.

http://www.htsmodelling.com/

مقالات منتشر شده

ARTICLE IN PRESS

Ceramics International xxx (xxxx) xxx–xxx

Contents lists available at ScienceDirect

Ceramics International

journal homepage: www.elsevier.com/locate/ceramint

Enhancement in the performance of BSCCO (Bi-2223) superconductor with functionalized TiO_2 nanorod additive

Hesam Fallah-Arani[a], Saeid Baghshahi[b,*], Arman Sedghi[b], Nastaran Riahi-Noori[a]

[a] Non-Metallic Materials Research Group, Niroo Research Institute (NRI), Tehran, Iran
[b] Department of Materials Engineering, Faculty of Engineering, Imam Khomeini International University, Qazvin, Iran

ARTICLE INFO

Keywords:
BSCCO
Superconducting features
TiO_2 nanorod
Pinning force
Microstructure

ABSTRACT

Using a sol-gel route, we produced $(Bi,Pb)_2Sr_2Ca_2Cu_3O_{10+\theta}$ (Bi-2223) specimens with the addition of titanium dioxide nanorods (TiO_2-NR) additive, with the aim of understanding the role of one-dimensional (1D) additives on the magnetic properties, flux pinning ability and microstructure of Bi-2223. TiO_2-NR was hydrothermally prepared through the two-step process. The Isocyanatopropyltrimethoxysilane (IPTMS) was employed as a surface modifier of TiO_2-NR. Based on FTIR spectra, successful connection between the surface of TiO_2-NR with IPTMS was approved. XRD patterns revealed that the structure of Bi-2223 as the main phase was maintained with the increase of TiO_2-NR. An enhancement in the vortex pinning and superconducting properties was obtained in the specimen with the 0.2 wt%. TiO_2-NR. The microstructure of the samples showed enough contact between the plate-shape BSCCO grains. By increase of TiO_2-NR content, grain connectivity and grain alignment slightly diminished. Among the samples, the one containing 0.2 TiO_2-NR showed the largest magnetic hysteresis curves and the highest critical current density (J_c) equal to 2.01×10^6 A/cm^2, comparable to the considerable results reported for Bi-2223. The possible flux pinning mechanisms predominant in this compound were evaluated, indicating that TiO_2-NR improved the pinning performance in Bi-2223.

1. Introduction

Superconducting behavior, the appearance of diamagnetic properties and zero resistance simultaneously, has rapidly been developed for a range of innovative technology applications in industrial areas [1,2] Superconductor-based products are zero resistance, reliable, efficient, environment-friendly and power quality materials compared to their conventional counterparts [3,4]. Nowadays, scientists focus on further implementation of Bi-based ceramics materials capabilities in heavy-industrial [5].

Superconducting materials are categorized into two main groups. The type-II superconductors (high-temperature cuprates), discussed in the present research, exhibit desirable properties due to smaller magnitude of energy losses, lower power consumption and large magnetic field-current capacity. Moreover, high temperature superconducting (HTS) materials are good candidates for many industrial applications such as underground tapes, generators, filters, magnets, detectors, transformers, energy storage, fault current limiter and magnetic separation due to cost-effective and easier attainability of the starting ceramic materials [6–8].

Considering the Cu-O planes species, BSCCO superconductors with $(BiPb)_2Sr_2Ca_{n-1}Cu_nO_{2n+4+\theta}$ general formula have two HTS phases with critical temperature values of Tc ≈ 110-100 K (Bi-2223, n = 3) and Tc ≈ 95-90 K (Bi-2212, n = 2) [9,10]. It should be noted that Bi-2223 is preferable to other kinds of BSCCO system for the fabrication of tapes and cables for industrial applications. The high purity synthesis of Bi-2223 phase is somehow challenging because of generation of other side products and the occurrence of highly complex reaction mechanisms. Bi-2223 phase requires a long synthesis time to form an suitable fraction of Bi-2223 in the final product because the formation kinetics of the this phase is slow [11,12].

Various methods. have been used for the fabrication of BSCCO superconductors samples [13,14]. The widely used method is the conventional solid state reaction. However, some wet method like sol-gel has several advantages over the solid state method, as follows: capability to generate complex inorganic materials, lower synthesis temperatures, shorter processing times, greater mixing of precursors at atomic scale and better control of particle size. Recent investigations have revealed that the drying condition, heat treatment status, concentration of mixture solution, the chelating groups, the pH value of sol and the addition of nano materials are significant parameters in the improvement of the microstructure and superconducting parameters of

* Corresponding author.
E-mail address: baghshahi@eng.ikiu.ac.ir (S. Baghshahi).

https://doi.org/10.1016/j.ceramint.2019.07.198
Received 2 June 2019; Received in revised form 16 July 2019; Accepted 16 July 2019

Please cite this article as: Hesam Fallah-Arani, et al., Ceramics International, https://doi.org/10.1016/j.ceramint.2019.07.198

BSCCO system [15–17].

Recently, nano ceramics have been applied in various fields of engineering and science because of their unique properties, encouraging the researchers to examine the role of nanoparticles additions for obtaining more appropriate properties [18–20]. Many investigations are being conducted and much effort is being devoted to studying the impacts of nano addition into the microstructure of superconductors, in hope of achieving higher critical current density (J_C) and superconducting temperature (Tc) [21–23]. In the recent years, considerable studies have been focused to the trends concerning the elevation of the Jc by creating efficient active pinning centers via substitutions and additions of nano-sized additives such as Co_3O_4, Au, Sm_2O_3, Al_2O_3, ZrO_2, Ag and etc [24–30]. It has been reported that nano sized particles can create strong pinning forces because of their sizes are around to the coherence length. Moreover, defects caused by energetic radiations in BSCCO system were detected to be effective in increament of pinning forces [31,32]. In several similar works, the effects of some other nano-additives were scrutinized [33–36]. However, there are not enough researches focusing on the effect of one-dimensional nano additives such as TiO_2 nanorods (TiO_2-NR) on the superconducting properties of BSCCO. Further defects such as dislocations and columnar defects can be created with the presence of a 1D addition, contributing to the improvement of Jc value. To the best of our knowledge, there is no detailed report about the TiO_2-NR as an additive to BSSCO bulk. TiO_2 as a ceramic material has high thermal and chemical stability and high transmittance in the visible spectral range. This material could be formed in three possible crystallographic phases, that is anatase, rutile, and brookite [37].

In this research, we aim to investigate the effect of TiO_2-NR as a new pinning center on superconducting, magnetic and electrical features of Bi-2223 synthesized by sol-gel route. Different parameters such as critical temperature (T_C), magnetic susceptibility (χ_{dc}(T)) and magnetization critical current density J_{cm} (H) were evaluated and compared. The pinning force was determined to illustrate the mechanism of pinning activated in the specimens.

2. Experimental procedure

2.1. Materials

Bi-based bulk samples with the chemical composition of $(Bi\text{-}Pb)_2Sr_2Ca_2Cu_3O_0 + xTiO_2$, where x = 0.0,0.2, 0.4 and 0.8 wt%, were prepared by sol-gel method using high purity powders of Bi $(NO_3)_3.5H_2O$, $Ca(NO_3)_2.4H_2O$, $Pb(NO_3)_2$, $Cu(NO_3)_2.3H_2O$ and Sr $(NO_3)_2$. Firstly, the proper amounts of metal nitrates were added in 50 ml of HNO_3 (0.1 M) and the resulting solution was stirred at 50 °C to obtain a light blue solution. To prepare stable metal chelate complexes (EDTA-metal cation), ethylenediaminetetraacetic acid (EDTA) and ammonium hydroxide were gradually added to the precursor solution and stirred at 80 °C. The polymerizing agent of Ethylene glycol (EG), with the molar EG/metal ions ratio of 3.5:1, was added to the solution, so that a dark blue solution was obtained. The concentrated solution was subsequently heated in an oil bath at about 200 °C to totally evaporate the solvent, producing a black foam-like mass after 10 h. Further heating at about 300 °C removed water and organic impurities, converting into the precursor powder. The remaining powder was mixed with TiO_2-NR and ground in an agate mortar for about half an hour. The obtained powder was calcined at 820 °C for 24 h to decompose the alkaline-earth carbonates. After cooling to room temperature, the calcined powders were removed from the furnace and was then ground by an agate mortar. The powders were pressed into pellets under pressure of 5 ton/cm^2 and sintered at 850 °C for 100 h in an air atmosphere.

2.2. Synthesis and surface modification of TiO_2 nanorods

TiO_2 nanorod was prepared via a two-step hydrothermal route as described elsewhere [38]. Briefly, 40 ml NaOH(10 M) was added into TiO_2 Degussa P25 nanoparticle (1 g) and stirred for 1 h. The homogeneous suspension was transferred to autoclave (100 ml) and hydrothermaled at 190 °C for 72 h in an oven. Then, the autoclave was allowed to be air-cooled to room temperature followed by rinsing of products with dilute HCl. In the next step, the residue was added into solution of 40 ml ethanol-water (20 ml: 20 ml) and dimethylamine (2 ml) accompanied with magnetic stirring for 1 h. The resulted solution was hydrothermally heated at 180 °C for 10 h. After vacuum filtration, the residue was finally dried, and the white-color TiO_2-NR powder was gained. The silane agent of 3-Isocyanatopropyltrimethoxysilane (IPTMS) was used for the surface modification of TiO_2. Synthesized TiO_2 nanorads were ultrasonically dispersed in distilled water at amplitude 30%, and the solution was mixed by IPTMS, followed by refluxing at 80°C for 5 h. The centrifugation of finalized solution was conducted for 10 min at 10000 rpm to separate TiO_2-NR from the solvent fallowed by washing two with ethanol to remove excess silane. The modified nanorods were finally dried at 100 °C for 12 h.

2.3. Characterization

X-ray diffraction (XRD) analysis and X'Pert Pro MPD (PANalytical) diffractometer operated with Cu-Kα radiation were used to explore the structural and phase composition. Besides, the XRD peaks observed allow us to calculate the relative volume fractions of the low-Tc and high-Tc phases ($f_{(2223)}$ and $f_{(2212)}$) using Eqs. (1) and (2) [39]:

$$f(2223) = \frac{\sum I_{2223\,(hkl)}}{\sum I_{2223\,(hkl)} + \sum I_{2212\,(hkl)} + \sum I_{others}} \quad (1)$$

$$f(2212) = \frac{\sum I_{2212\,(hkl)}}{\sum I_{2223\,(hkl)} + \sum I_{2212\,(hkl)} + \sum I_{others}} \quad (2)$$

Here $I_{2223\,(hkl)}$ and $I_{2212\,(hkl)}$ relate to the intensity of the Bi-2223 and Bi-2212 peak, respectively. FTIR spectroscopy (8500S SHIMADZU) was applied to verify functional groups forming on TiO_2-NR surface. Fractured surface morphology is investigated with the aid of FESEM (Tescan Mira3). Energy-dispersive X-ray spectroscopy (EDS) analysis system was performed to study the relative content of the specimen. Additionally, magnetization measurements were executed using a SQUID magnetometer to calculate the magnetization critical current density (J_c) values, by using extended Bean's model the (Eq. (3)) [28]:

$$Jc = 30\frac{\Delta M}{d} \quad (3)$$

Here d represents the thickness of the specimens and $\Delta M = \Delta M = M^+ - M^-$ is calculated from the hysteresis loop.

3. Results and discussion

3.1. Grafting process

Fig. 1 shows the process of TiO_2-NR with IPTMS surface modifier. As can be seen in Fig. 1, the process of TiO_2-NR grafted IPTMS are involved, three stages of hydrolysis, condensation reaction and bond formation.

As shown in Fig. 2, isocyanate groups (-NCO) react with the silanol groups (R_3SiOH) produced during hydrolysis. It is noticed that the cross linked polymer structure was formed on the TiO_2-NR through a subsequent condensation of IPTMS. It should be noted that -NH_2 groups and CO_2 were formed as a result of the reactivity of water and -NCO. Therefore, the NH_2 are only present at the surface of TiO_2-NR. The successive condensation of hydrolyzed IPTMS are interrupted to develop the cross linked network [40,41].

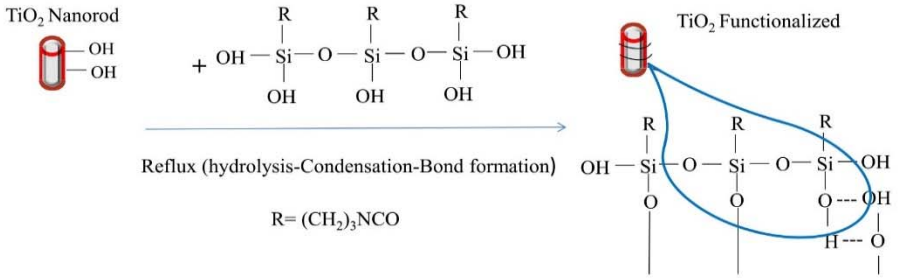

Fig. 1. Reaction scheme for TiO_2-NR surface modification.

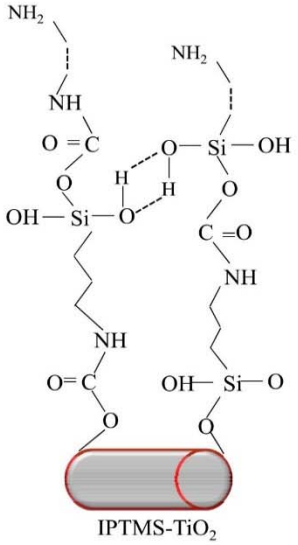

Fig. 2. Cross linked network generated on TiO_2-NR.

Table 1
Characteristic bonds in infrared spectra of IPTMS- TiO_2.

No.	Wavenumber (cm^{-1})	Functionality
1	≤700	Main characteristic peaks of titania bonds (Ti–O–Ti & Ti–O)
2	910–940	Stretching vibration band of Ti–O–Si
3	1040	Si-*O*-Si bond (condensation reaction between silanol groups)
4	1550	NHCO groups
5	1560–1610	N-H bending vibration of amines (-NH_2)
6	1640	Characteristic peaks of hydroxyl groups
7	2800 & 2900	Methylene group (C–H symmetrical stretching vibration)
8	3200–3400	Characteristic peaks of hydroxyl groups

3.2. FTIR spectroscopy

Fig. 3 shows infrared spectra of IPTMS-TiO_2 and untreated TiO_2-NR. The main FTIR bands of the IPTMS-TiO_2 are presented in Table 1.

In the spectrum of IPTMS-grafted TiO_2, the bands lower 700 cm^{-1} are assigned to the bonding of titania [41]. Furthermore, the broad peak at region 3400 and 3200 cm^{-1} peak and the peak at 1640 cm^{-1} appearing in this spectrum confirms the presence of surface hydroxyl groups (-OH). The bands at 2900 and 2800 cm^{-1} can be attributed to methylene group and the C-H bond [42].

The existence of the 1040 cm^{-1} peak related to the Si-O-Si bond confirms that the condensation reaction occurred between silanol groups. Furthermore, the bond of N-H bending of primitive -NH_2 was observed at the region 1610–1560 cm^{-1}. As seen in Fig. 2, amine species was only in the outermost layer of IPTMS-TiO_2. In infrared spectra, the intensity of amines was low and overlapped with that of OH groups. The peak corresponding to NHCO groups was observed at 1550 cm^{-1} revealing the reaction between -NCO and -OH groups. Moreover, the absorption from 910 to 940 cm^{-1} was caused by the vibration of Ti-O-Si, indicating the reaction between -OH group of TiO_2 and R_3SiOH. Since the washing or centrifugal separation will remove physical adsorbed and residual (non-reacted) IPTMS agent. It should be noted, existence of the OH groups on the surface of the TiO_2-NR (TiOH) leads to the formation of active cases for the reaction with silane groups. The mentioned peaks illustrate that successful surface modification of TiO_2-NR has occurred [40,43].

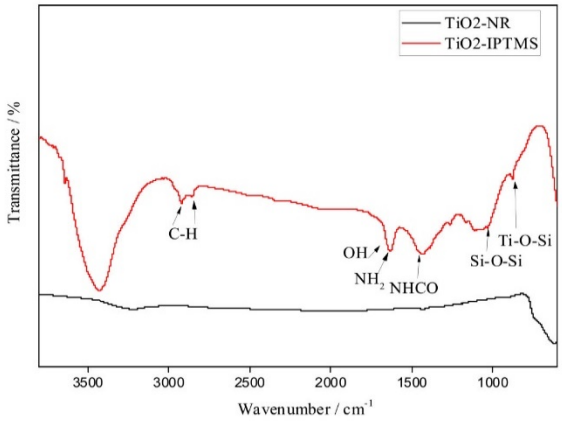

Fig. 3. FTIR of (a) untreated TiO_2 and (b) IPTMS-grafted TiO_2.

3.3. Phase analysis

Fig. 4 shows the XRD patterns of Bi-2223 specimens sintered with various TiO_2-NR contents. The analyses of XRD patterns indicated that all samples were composed of Bi-2223 as the principal phase and Bi-2212 and Bi-2201 as the ordinary phases.

As the mounts of TiO_2-NR increased, the Bi-2223 decreased and the optimum TiO_2-NR content for the samples, to achieve a great volume fraction of Bi-2223 is x = 0.2 wt%. It seems that the addition of a high

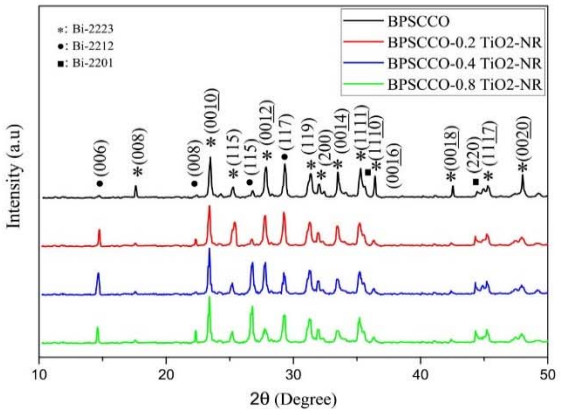

Fig. 4. XRD patterns of Bi2223 sintered with varous concentration of TiO_2 nanorods.

Table 2
Lattice parameters of the Bi-2223-X (wt%) TiO_2-NR unit cell and T_C values obtained from susceptibility-temperature for all samples (0–0.8).

Sample	Lattice parameters		T_{cj} (K) (intergranular transition)	T_c (K) (intragranular transition)
X(wt %)TiO_2-NR	a ≈ b(Å)	c(Å)		
0.0	3.823(1)	37.074(4)	———	110.9
0.2	3.823(2)	37.074(2)	———	112.5
0.4	3.823(4)	37.074(1)	99.2	109.1
0.8	3.823(3)	37.074(1)	97.1	107.3

TiO_2 concentration can affect the rate of reaction, which restricts slightly the formation of Bi-2223. This fact suggests that the TiO_2-NR addition leads to a change in the homogeneity of the transient liquid forming, its viscosity and the reaction rate of the Bi- 2223 phase. According to the XRD spectra, peaks assigned to the TiO_2 phase admixture was not detected even with high TiO_2-NR amounts. Moreover, after the Rietveld refinements, the lattice parameters are obtained, as listed in Table 2. As shown in Table 2, no significant change in lattice parameters is observed. It is significant to note that for all samples, the structure of sintered samples did not depend on TiO_2–NR addition, implying TiO_2-NR did not fit into the structure of Bi-2223. The lattice parameter values are in accordance with those reported by other [13,44].

3.4. Microstructural analysis

Fig. 5 shows the FESEM micrograph of TiO_2-NR, which were used as an additive and the fractured surface of Bi-2223 matrix sintered at 850 °C. The rods appear relatively uniform with micron-sized lengths and about 70 nm diameter (Fig. 5a). As shown in Fig. 5b, the typical microstructure of Bi-2223 superconductors, which is flaky layers of plate-like grains.

The FESEM images of TiO_2-NR added samples (x = 0.2 and x = 0.8) are shown in Fig. 6. From the photographs, we can see that the granular structure of samples having randomly aligned plate-shape grains and porous within BSCCO grains.

However, it is clear from the micrographs that no significant variation of microstructure occurs with the presence of TiO2. However, the average grain size in the samples with lower TiO_2 content is slightly larger. Furthermore, orientation and connectivity of superconductors grains are slightly worsened in x = 0.8 sample. It is significant to emphasize that TiO_2-NR entities reside in the grain boundaries and fill the pores inside the grains. It is suggested that such a microstructure may lead to a variation in connecting region and grain boundary content because of the existence of effective centers for pinning in the BSCCO matrix.

Fig. 7 present the elemental mapping of the $Bi_2Sr_2Ca_2Cu_3O_6$ + TiO_2 NR sample, indicating that superconductors grains consist of Bi, Ca, Cu, Pb, Sr, O and Ti element of TiO_2 nanorods.

3.5. Magnetic features

Fig. 8 depicts the magnetic susceptibility (χ_{dc}) against temperature for various added samples. As shown in Fig. 8, the onset of the transition temperature values, T_c, varied by the addition of TiO_2-NR. Initially, T_c raised with the enhancement of TiO_2-NR content up to 0.2, and then further TiO_2-NR addition reduced T_c.

The reduction of Tc can be attributed to strain accumulation at the interface of TiO_2-NR/Bi2223. In other words, distorted regions near the interface are considered to be responsible for superconductivity degradation due to a substantial change in the carrier density. The 0.2 wt % nanorods added sample, Compared with Bi2223 sample, possesses higher T_c and larger negative magnetization (Fig. 8), indicating the existence of small concentrations of TiO_2-NR results in an enhancement in Bi-2223 grains connectivity.

According to the χ-T graphics observed, a typical single-step transition peak is seen for x = 0.0 and x = 0.2 specimens. This trend is a characteristic feature of pure superconductors followed by a continuous decrement in susceptibility value with temperature. In x = 0.4 and x = 0.8 samples, a second peak becomes manifest at T_{cj} ~ 97 °C. The main reason for the appearance of the second peak is the formation of Bi-2212 or other phases which are detected by XRD measurement. It is obvious from Table 1 that the minimum Tc (107.3 K) and T_{cj} (97.1 K) values belong to the worst sample (x = 0.8), whereas the maximum value of Tc = 112.5 K is observed in the best sample (x = 0.2). According to the obtained results, the TiO_2-NR addition affects the weak links, intergranular connectivity, grain orientations, grain morphology, local structural distortions, defects and disorders. These findings are in excellent agreement with FESEM micrographs and XRD patterns explained previously, which clarified that 0.2 wt% TiO_2 NR sample possesses the best grain size and coupling.

To identify the effect of TiO_2 addition and to determine vortex flux pinning mechanisms, the intra-granular features of products were investigated. Fig. 9 presents the hysteresis curves for 0.0–0.8 wt% TiO_2–NR added products, at 10 K.

Obviously, the TiO_2–NR addition cause considerable variations in the size of the magnetic hysteresis. Among all samples, the hysteresis loop area is the highest for the samples containing a low concentration of TiO2 –NR (0.2 wt%). As shown in Fig. 9, the magnetization values and the hysteresis loop width increased as the TiO2 –NR concentration increased up to 0.2 wt% and then it started to decrease for higher TiO2 –NR concentrations. The enhancement in the width of hysteresis loops can be attributed to the improvement of grain morphology and creating pinning centers when appropriate defects form in the matrix. The mentioned results indicated that the TiO2 –NR have efficiently contributed to the enhancement of flux pinning, creating pinning centers and causing the improvement of grain morphology when suitable phases form in the Bi-2223.

Fig. 10a displays intragranular J_c (H) for all products, at 10 K, achieved from the magnetic hysteresis curves. It can be seen that TiO_2 concentration and the applied magnetic field affect J_c values. TiO_2-NR in small amount, compared with the non-added samples, contributes to the mechanism of vortex pinning, increasing J_c values. Note that J_c can be influenced by artificial pinning centers due to the presence of nanorods. The highest J_C values have been obtained in (x = 0.2) TiO_2-NR sample, 2.01 × 10^6 A/cm^2 at 10K. The reason can be illustrated as the result of the enhancement of grains connectivity and grain alignment, which is in accordance with the results obtained from FESEM images.

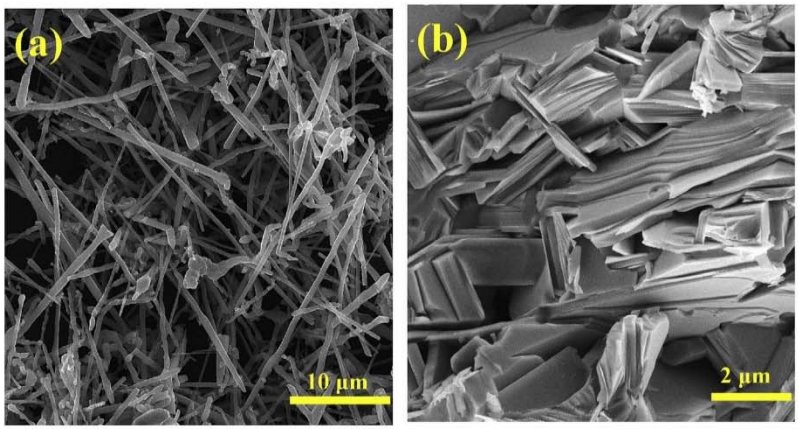

Fig. 5. FESEM micrographs of a)TiO_2 nanorods addition and b) Bi-2223 sintered at 850 °C.

The large and well oriented grains can be associated with the reduction in the grain boundaries and a decrement of adjoining grains angle, resulting in a higher current. By the increasing of TiO_2-NR addition, J_C values decreased, indicating the deterioration of connection between the grains and mechanism of pinning due to misorientation of the grains and raise of the local structural distortions, weak-links, lattice strains and porosity. The J_c findings enable us to gain further insight into the origin of enhanced pinning features and estimate the pinning force density (Fp) by Fp = Jc × B [45].

Fig. 10b shows the pinning force density all samples at 10K. Notably, the flux pinning strength depends on the number of pinning centers, morphology and size. As shown in Fig. 10b, the maximum field (H_{max}) and the maximum force ($F_{P\text{-}max}$) is higher in x = 0.2 sample compared to other ones, as depicted in Fig. 10b. The H_{max} corresponds to the magnetic field at which the F_P attains its maximum. It should be noted that a larger H_{max} indicates stronger pinning strength and the better performance in the x = 0.2 sample is partly caused by the enhancement of H_{max}. In this case, H_{max} and $F_{P\text{-}max}$ decrease with the increase of TiO_2-NR, indicating a decrease in flux pinning with TiO_2-NR. It is worth mentioning that such an enhancement in the pinning obtained by the only 0.2 wt% nanorods. Therefore, it is now clear that the flux pinning strength can be modified by determining the added material as pinning centers and its appropriate concentration. The result of this study reveals a high efficiency of flux pinning by nanorods.

To determine the pinning mechanisms, normalized magnetic field ($h = H/H_{max}$) dependence of flux pinning strength ($f_p = F_P/F_{P\text{-}max}$) was studied. The experimental data of f_p-h is often construed according to Eqs. (4)–(6) [46,47].

$$f(h) = \frac{9h}{4}\left(1 - \frac{h}{3}\right)^2 \qquad \textit{normal point pinning} \tag{4}$$

$$f(h) = \frac{25}{16}\sqrt{h}\left(1 - \frac{h}{5}\right)^2 \qquad \textit{surface pinning} \tag{5}$$

$$f(h) = 3h^2\left(1 - \frac{2h}{3}\right) \qquad \textit{Δκ pinning} \tag{6}$$

Fig. 11 shows fp versus h plots for all the samples. The plots for the experimental and theoretical data according to Eqs (4)–(6) are shown in the figure to examine the flux strength. For fields below and beyond h_{max}, the position of data are between point and surface pinning and in near h_{max}, the data are scattered between point and *Δκ* pinning. We cannot conclude the presence of Δκ pinning because of the limitation of data above h_{max}. Whereas, the comparison of theoretical date of fp and experimental plots in sample with nanorod indicates the activation of surface and point mechanisms due to crossing between TiO_2-NR and vortices. At low field, the surface of well-aligned superconductor grains treats as a pinning center. This finding reveals that the existence of TiO_2-NR additive amplifies the contribution of pinning centers in flux

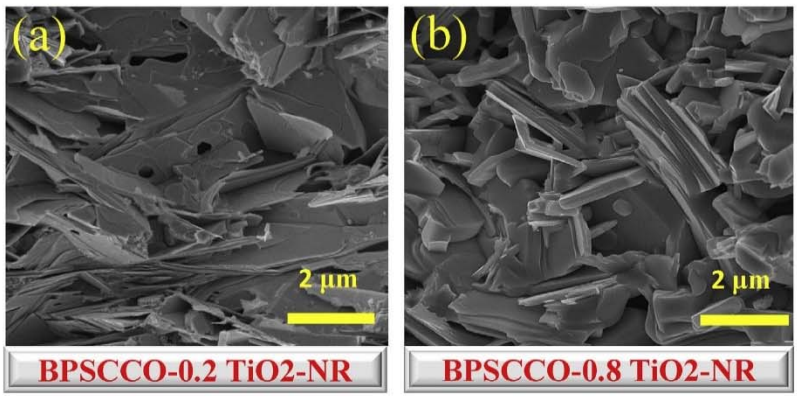

Fig. 6. FESEM images of specimens sintered with various concentration of TiO_2 nanorods.

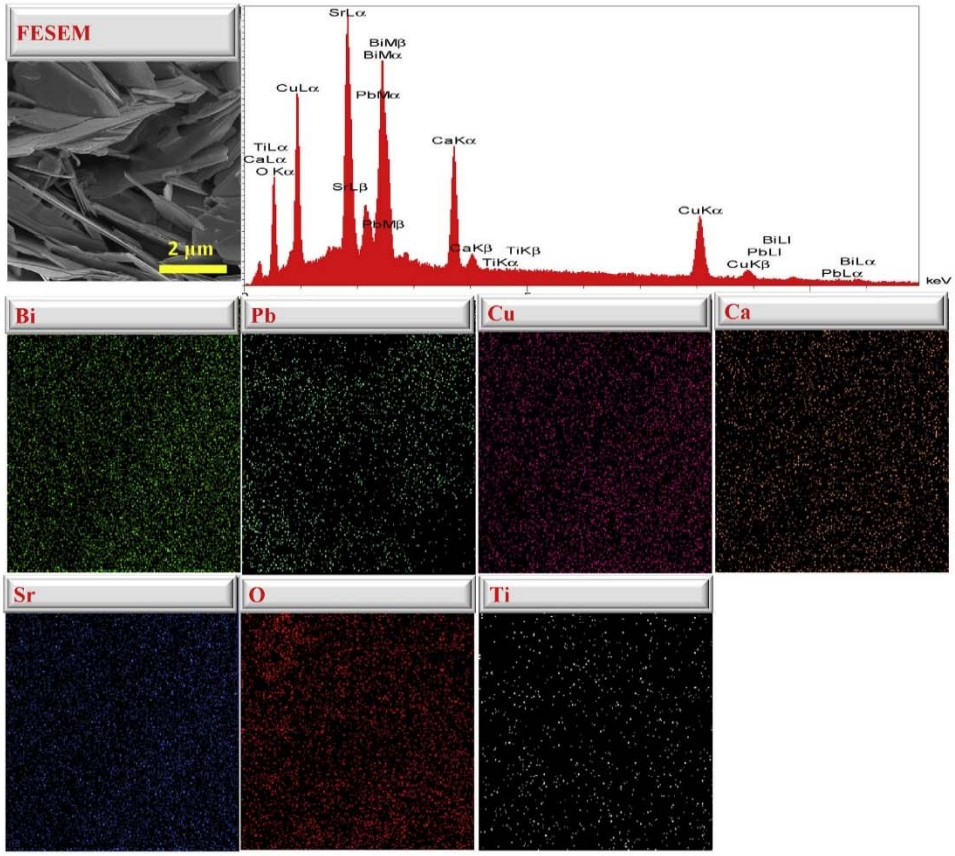

Fig. 7. Elemental mapping for Bi-2223 $^{-}$ TiO_2-NR.

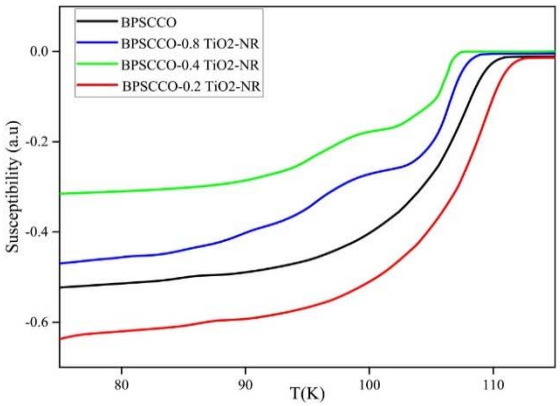

Fig. 8. Variation of susceptibility over temperature curves in 10 Oe.

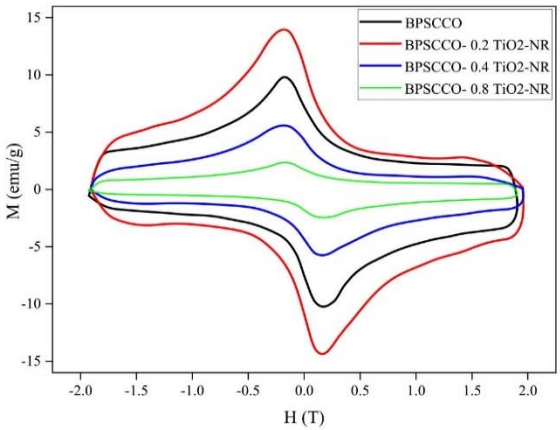

Fig. 9. Magnetization hysteresis curves (M(H)) at 10 K for all TiO_2-NR added products.

pinning features.

4. Conclusion

In this paper, the impact of TiO_2-NR on the superconducting properties and flux pinning features of Bi-2223 superconductors was investigated. The XRD result confirmed the formation of the high Tc phase of Bi-2223 accompanied by the relatively small concentration of

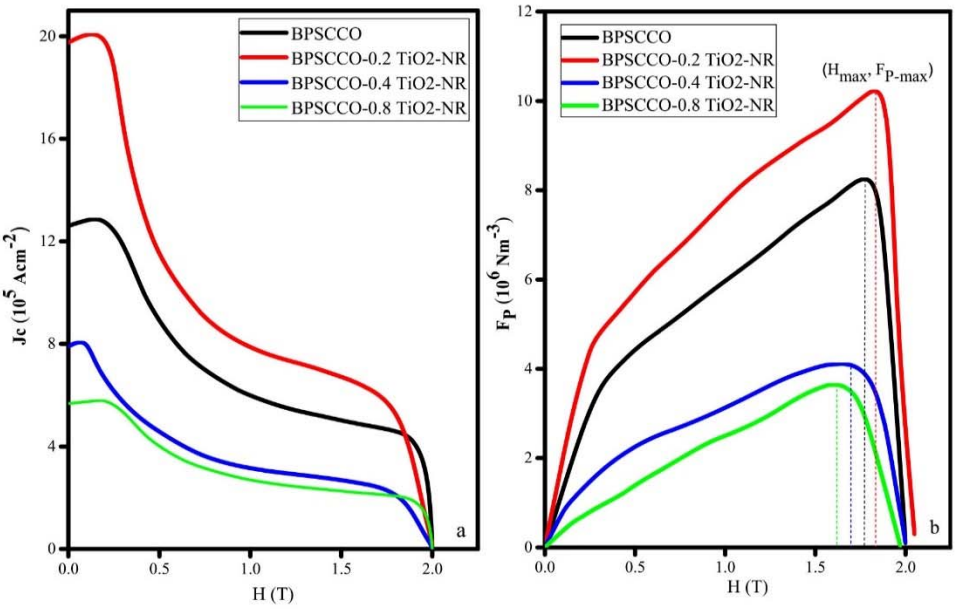

Fig. 10. a) Critical current at 10 K and b) Magnetic field dependencies of Fp for 0.0 wt% - 0.8 wt%TiO_2-NR added samples.

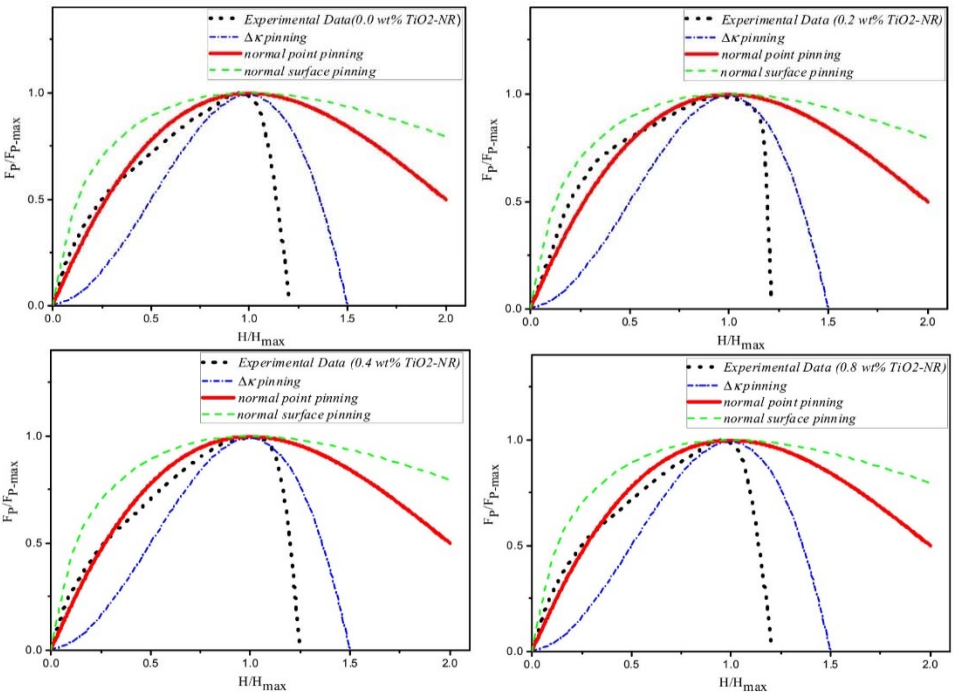

Fig. 11. Normalized pinning force versus the normalized magnetic field for all specimens. Doted (blue), solid (red) and dashed (green) lines represent the theoretical plots based on Eqs. (4)–(6) respectively. (For interpretation of the references to color in this figure legend, the reader is referred to the Web version of this article.)

Bi-22212 phase at the specimen with 0.2 wt% TiO_2-NR content. From FESEM/EDX observation, it was concluded that no significant variation of microstructure occurs with the presence of TiO_2-NR. However, grain characteristics such as connectivity and alignment are slightly worsened in x = 0.8 specimen. Based on magnetic measurements, the highest values of T_c and J_c corresponded to the 0.2 wt% TiO_2-NR samples. The $F_{P\text{-}max}$ and H_{max} were higher in the 0.2 wt% TiO_2-NR specimen compared to the other ones. In addition, the hysteresis curve obtained for this specimen had the highest width and magnetization value, and the width of hysteresis loops decreased with the TiO_2-NR increased. Therefore, the results proved a high efficiency of flux pinning in Bi-2223 ceramic materials by TiO_2-NR

References

[1] A.T. Ulgen, T. Turgay, C. Terzioglu, G. Yildirim, M. Oz, Role of Bi/Tm substitution in Bi-2212 system on crystal structure quality, Pair wave function and polaronic states 764 (2018) 755–766, https://doi.org/10.1016/j.jallcom.2018.06.142.

[2] A. Costa, F.M., N.M. Ferreira, S. Rasekh, A.J.S. Fernandes, M.A. Torres, M.A. Madre, J.C. Diez, Sotelo, Very large superconducting currents induced by growth tailoring, Cryst. Growth Des. 15 (2015) 2094–2101, https://doi.org/10.1007/978-3-642-19971-4.

[3] B. Wang, Y. Ren, Z. Deng, J. Zheng, W. Zhang, J. Zhang, X. Zheng, A high-temperature superconducting maglev-evacuated tube transport (HTS maglev-ETT) test system, IEEE Trans. Appl. Supercond. 27 (2017) 1–8, https://doi.org/10.1109/tasc.2017.2716842.

[4] Haizhen Wang, Jingyin Zhang, Xiaoye Niu, Bo Tian, Hong Hui, Ying Xin, Electrical insulation of HTS coils in saturated iron core superconducting fault current limiter, IEEE Trans. Appl. Supercond. 24 (2014) 1–4, https://doi.org/10.1109/TASC.2013.2290944.

[5] R.S. Dondapati, A. Kumar, G.R. Kumar, P.R. Usurumarti, S. Dondapati, Superconducting magnetic energy storage (SMES) devices integrated with resistive type superconducting fault current limiter (SFCL) for fast recovery time, J. Energy Storage. 13 (2017) 287–295, https://doi.org/10.1016/j.est.2017.07.005.

[6] G. Yildirim, Determination of optimum diffusion annealing temperature for Au surface-layered Bi-2212 ceramics and dependence of transition temperatures on disorders, J. Alloy. Comp. 699 (2017) 247–255, https://doi.org/10.1016/j.jallcom.2016.12.370.

[7] Y. Zalaoglu, F. Karaboga, C. Terzioglu, G. Yildirim, Improvement of mechanical performances and characteristics of bulk Bi-2212 materials exposed to Au diffusion and stabilization of durable tetragonal phase by Au, Ceram. Int. (2017) 0–1, https://doi.org/10.1016/j.ceramint.2017.02.104.

[8] S. Safran, H. Ozturk, F. Bulut, O. Ozturk, The influence of re-pelletization and heat treatment on physical , superconducting , magnetic and micro-mechanical properties of bulk BSCCO samples prepared by ammonium nitrate precipitation method, Ceram. Int. (2017) 1–7, https://doi.org/10.1016/j.ceramint.2017.08.114.

[9] Y. Zalaoglu, C. Terzioglu, T. Turgay, G. Yildirim, Detailed survey on minimum activation energy for penetration of Ni nanoparticles into Bi-2223 crystal structure and temperature-dependent Ni diffusivity, J. Mater. Sci. Mater. Electron. 29 (2018) 3239–3249, https://doi.org/10.1007/s10854-017-8259-6.

[10] H. Fallah-Arani, S. Baghshahi, A. Sedghi, D. Stornaiuolo, F. Tafuri, N. Riahi-Noori, Enhancement in superconducting properties of $Bi_2Sr_2Ca_1Cu_2O_{8+\theta}$ (Bi-2212) by means of boron oxide additive, Phys. C Supercond. Its Appl. 548 (2018) 31–39, https://doi.org/10.1016/j.physc.2018.01.012.

[11] H. Fallah-arani, A. Sedghi, S. Baghshahi, N. Riahi-Noori, H. Koohani, Enhancement of superconducting properties in Bi-Pb-Sr-Ca-Cu-O system, 31 Th Int. Power Syst. Cnference. 2016, pp. 64–76.

[12] N.G. Margiani, G.A. Mumladze, N.A. Papunashvili, Z.A. Adamia, D.I. Dzanashvili, Effect of BN-added precursors on phase formation and transport properties of (Bi,Pb)-2223 HTS, J. Supercond. Nov. Magnetism 27 (2014) 397–400, https://doi.org/10.1007/s10948-013-2330-1.

[13] H. Fallah-Arani, S. Baghshahi, A. Sedghi, D. Stornaiuolo, F. Tafuri, D. Massarotti, N. Riahi-Noori, The influence of heat treatment on the microstructure, flux pinning and magnetic properties of bulk BSCCO samples prepared by sol-gel route, Ceram. Int. 44 (2018) 5209–5218, https://doi.org/10.1016/j.ceramint.2017.12.128.

[14] G. Kirat, O. Kizilaslan, M.A. Aksan, Effect of the Er-substitution on critical current density in glass-ceramic $Bi_2Sr_2Ca_2Cu_{3-x}Er_xO_{10+\delta}$ superconducting system, Ceram. Int. 42 (2016) 15072–15076, https://doi.org/10.1016/j.ceramint.2016.06.171.

[15] H. Yang, M.B. Shahzad, X. Yu, Y. Qi, Influence mechanism of secondary gel technique on Bi-2212 superconducting phase : gel model simulation and verification, Mater. Des. 99 (2016) 115–119, https://doi.org/10.1016/j.matdes.2016.03.051.

[16] D.C. Green, R. Boston, S. Glatzel, M.R. Lees, S.C. Wimbush, J. Potticary, W. Ogasawara, S.R. Hall, On the mechanism of cuprate crystal Growth : the role of mixed metal carbonates, Adv. Funct. Mater. 25 (2015) 4700–4707, https://doi.org/10.1002/adfm.201501058.

[17] M.E. Kir, B. Özkurt, M.E. Aytekin, The effect of K-Na co-doping on the formation and particle size of Bi-2212 phase, Phys. B Condens. Matter 490 (2016) 79–85, https://doi.org/10.1016/j.physb.2016.03.016.

[18] H.F. Arani, A.R. Mirhabibi, S. Collins, R. Daroughegi, A. Khalife Soltani, R. Naghizadeh, N. Riahi-Noori, R. Aghababazadeh, A. Westwood, Enhancement in graphitization of coal tar pitch by functionalized carbon nanotubes, RSC Adv. 7 (2017) 5533–5540, https://doi.org/10.1039/C6RA25441A Effect of Nano Carbon Additives on the Microstructure of Polyvinyl Chloride Heated up to 2000°C, 4046.

[19] H.F. Arani, A. Mirhabibi, Effect of nano carbon additives on the microstructure of polyvinyl chloride heated up to 2000°C, Fullerenes, Nanotubes, Carbon Nanostruct. 24 (1) (2016) 34–42, https://doi.org/10.1080/1536383X.2015.1110696.

[20] G.P. Pepe, D. Montemurro, D. Stornaiuolo, L. Galletti, G. Rotoli, F. Lombardi, D. Massarotti, A. Tagliacozzo, H.F. Arani, L. Parlato, B. Jouault, F. Tafuri, G. Campagnano, P. Lucignano, R. Caruso, L. Longobardi, What happens in Josephson junctions at high critical current densities, Low Temp. Phys. 43 (2017) 816–823, https://doi.org/10.1063/1.4995630.

[21] K. Matsumoto, P. Mele, Artificial pinning center technology to enhance vortex pinning in YBCO coated conductors, Supercond. Sci. Technol. 23 (2010), https://doi.org/10.1088/0953-2048/23/1/014001.

[22] Y. Slimani, E. Hannachi, A. Ekicibil, M.A. Almessiere, F. Ben Azzouz, Investigation of the impact of nano-sized wires and particles TiO_2 on Y-123 superconductor performance, J. Alloy. Comp. 781 (2019) 664–673, https://doi.org/10.1016/j.jallcom.2018.12.062.

[23] E. Hannachi, Y. Slimani, F. Ben Azzouz, A. Ekicibil, Higher intra-granular and inter-granular performances of YBCO superconductor with TiO_2 nano-sized particles addition, Ceram. Int. 44 (2018) 18836–18843, https://doi.org/10.1016/j.ceramint.2018.07.118.

[24] O.V.S., L.M.G., J.S., T.N. Smirnova, Surface modified ZrO_2 and TiO_2 nanoparticles embedded in organic photopolymers for highly effective and UV-stable volume holograms, Nanotechnology 18 (2007) 105704, https://doi.org/10.1088/0957-4484/18/10/105704.

[25] H. Baqiah, S.A. Halim, M.I. Adam1, S.K. Chen, S.S.H. Ravandi, M.A.M. Faisal, The effect of magnetic nanoparticle addition on the superconducting properties of $Bi_{1.6}Pb_{0.4}Sr_2Ca_2Cu_3O_8$ superconductors, Solid State Sci. Technol. 17 (2009) 81–88.

[26] F. Ben Azzouz, M. Annabi, M. Zouaoui, M. Ben Salem, Effects of Al_2O_3 nanometer particles addition on the fluctuation conductivity in (Bi,Pb)-2223 superconductors, Phys. Status Solidi Curr. Top. Solid State Phys. 3 (2006) 2978–2981, https://doi.org/10.1002/pssc.200567008.

[27] A. Ghattas, M. Annabi, M. Zouaoui, F. Ben Azzouz, M. Ben Salem, Flux pinning by Al-based nano particles embedded in polycrystalline (Bi,Pb)-2223 superconductors, Phys. C Supercond. Its Appl. 468 (2008) 31–38, https://doi.org/10.1016/j.physc.2007.10.006.

[28] H. Xian, T. Peng, H. Sun, J. Wang, Preparation, characterization and super-capacitive performance of graphene nanosheets from microcrystalline graphite, J. Mater. Sci. Mater. Electron. 26 (2014) 242–249, https://doi.org/10.1007/s10854-014-2391-3.

[29] S.F. Oboudi, M.Q. Mustafa, Synthesis and characterization of Ag nanoparticles addition on BPSCCO superconducting thin films, Adv. Nanoparticles 5 (2016) 75–82.

[30] N.K. Saritekin, M. Pakdil, E. Bekiroglu, G. Yildirim, Examination of effective nucleation centers for flux pinning of vortices and optimum diffusion annealing temperature for Au-diffusion-doped Bi-2212 polycrystalline compound, J. Alloy. Comp. 688 (2016) 637–646, https://doi.org/10.1016/j.jallcom.2016.07.203.

[31] S. Horii, K. Yamada, H. Kai, A. Ichinose, M. Mukaida, Introduction of c -axis-correlated 1D pinning centers and vortex Bose glass in Ba–Nb–O-doped $ErBa_2Cu_3O_y$ films, 1115 (n.d.). doi:10.1088/0953-2048/20/12/005.

[32] A. Crisan, V.S. Dang, P. Mikheenko, Nano-engineered pinning centres in YBCO superconducting films, Phys. C Supercond. Its Appl. 533 (2017) 118–132, https://doi.org/10.1016/j.physc.2016.06.011.

[33] T. Matsushita, H. Nagamizu, K. Tanabe, M. Kiuchi, E.S. Otabe, H. Tobita, M. Yoshizumi, T. Izumi, Y. Shiohara, D. Yokoe, T. Kato, T. Hirayama, Improvement of flux pinning performance at high magnetic fields in $GdBa_2Cu_3O_y$ coated conductors with BHO nano-rods through enhancement of BC_2, Supercond. Sci. Technol. 25 (2012), https://doi.org/10.1088/0953-2048/25/12/125003.

[34] P. Yang, C.M. Lieber, Creation of strong-pinning columnar defects in nanorod/superconductor composites, J. Mater. Res. (1997) 16–18, https://doi.org/10.1557/JMR.1997.0393.

[35] Y.C. Guo, Y. Tanaka, T. Kuroda, S.X. Dou, Z.Q. Yang, Addition of nanometer SiC in the silver-sheathed Bi2223 superconducting tapes, Phys. C Supercond. 311 (1999) 65–74 1-2.

[36] Y. Slimani, M.A. Almessiere, E. Hannachi, M. Mumtaz, A. Manikandan, A. Baykal, F. Ben Azzouz, Improvement of flux pinning ability by tungsten oxide nanoparticles added in $YBa_2Cu_3O_y$ superconductor, Ceram. Int. 45 (2019) 6828–6835, https://doi.org/10.1016/j.ceramint.2018.12.176.

[37] D. Dastan, N.B. Chaure, Influence of surfactants on TiO_2 nanoparticles grown by sol-gel technique, Int. J. Mater. Mech. Manuf. 2 (2014) 21–24, https://doi.org/10.7763/IJMMM.2014.V2.91.

[38] R. Siavash, G. Kia, L. Goh, A. Dolati, M. Ghorbani, Applied Catalysis B : environmental Sunlight-driven photoelectrochemical sensor for direct determination of hexavalent chromium based on Au decorated rutile TiO_2 nanorods, Appl. Catal. B Environ. 201 (2017) 411–418, https://doi.org/10.1016/j.apcatb.2016.08.026.

[39] G. Yildirim, M. Dogruer, F. Karaboga, C. Terzioglu, Formation of nucleation centers for vortices in Bi-2223 superconducting core by dispersed Sn nanoparticles, J. Alloy. Comp. 584 (2014) 344–351, https://doi.org/10.1016/j.jallcom.2013.08.150.

[40] S. Kango, S. Kalia, A. Celli, J. Njuguna, Y. Habibi, R. Kumar, Surface modification of inorganic nanoparticles for development of organic-inorganic nanocomposites - a review, Prog. Polym. Sci. 38 (2013) 1232–1261, https://doi.org/10.1016/j.progpolymsci.2013.02.003.

[41] X. Pan, Y. Zhao, S. Liu, C.L. Korzeniewski, S. Wang, Z. Fan, Comparing graphene-TiO_2 nanowire and graphene-TiO_2 nanoparticle composite photocatalysts, ACS Appl. Mater. Interfaces 4 (2012) 3944–3950, https://doi.org/10.1021/am300772t.

[42] J. Zhao, M. Milanova, M.M.C.G. Warmoeskerken, V. Dutschk, Surface modification

of TiO2 nanoparticles with silane coupling agents, Colloids Surfaces A Physicochem. Eng. Asp. 413 (2012) 273–279, https://doi.org/10.1016/j.colsurfa.2011.11.033.

[43] I. a. Janković, Z.V. Šaponjić, M.I. Čomor, J.M. Nedeljković, Surface modification of colloidal TiO_2 nanoparticles with bidentate benzene derivatives, J. Phys. Chem. C 113 (2009) 12645–12652, https://doi.org/10.1021/jp9013338.

[44] U. Öztornaci, B. Özkurt, The effect of nano-sized metallic Au addition on structural and magnetic properties of $Bi_{1.8}Sr_2Au_xCa_{1.1}Cu_{2.1}O_y$ (Bi-2212) ceramics, Ceram. Int. 43 (2016) 4545–4550, https://doi.org/10.1016/j.ceramint.2016.12.109.

[45] D. Sharma, R. Kumar, V.P.S. Awana, DC and AC susceptibility study of sol–gel synthesized $Bi_2Sr_2CaCu_2O_{8+d}$ superconductor, Ceram. Int. 39 (2013) 1143–1152, https://doi.org/10.1016/j. sacrament.2012.07.038.

[46] A. Biju, U. Syamaprasad, S. Vinu, R. Shabna, P.M. Sarun, Enhancement of flux pinning and Anderson–Dew-Hughes pinning analysis in $Bi_{1.6}Pb_{0.5}Sr_{2-x}Tb_xCa_{1.1}Cu_{2.1}O_{8+\delta}$ superconductor, J. Alloy. Comp. 477 (2008) L13–L16, https://doi.org/10.1016/j.jallcom.2008.10.033.

[47] P. Yin, R. Xiao, X. Xu, T. Duan, Z. Wang, Flux pinning properties in $BaPb_{0.77}Bi_{0.23}O_{3-\delta}$ compound, Phys. C Supercond. Its Appl. 542 (2017) 23–27, https://doi.org/10.1016/j.physc.2017.09.001.